



Support enhanced α -pinene isomerization over HPW/SBA-15

Lucia Frattini, Mark A. Isaacs, Christopher M.A. Parlett, Karen Wilson, Georgios Kyriakou, Adam F. Lee*

European Bioenergy Research Institute, Aston University, Aston Triangle, Birmingham B4 7ET, UK

ARTICLE INFO

Article history:

Received 10 May 2016

Received in revised form 21 June 2016

Accepted 25 June 2016

Available online 27 June 2016

Keywords:

Heteropolyacid

SBA-15

α -Pinene

Phosphotungstic acid

ABSTRACT

A family of mesoporous SBA-15 supported $\text{H}_3\text{PW}_{12}\text{O}_{40}$ (HPW) catalysts were synthesized by wet-impregnation and compared with fumed silica analogues for the solventless isomerization of α -pinene under mild conditions. Structural and acidic properties of supported HPW materials were characterized by powder XRD, HRTEM, XPS, TGA, N_2 porosimetry, DRIFTS, and ammonia and propylamine chemisorption and TPD. The high area, mesoporous SBA-15 architecture facilitates the formation of highly dispersed (isolated or low dimensional) HPW clusters and concomitant high acid site densities (up to 0.54 mmol g^{-1}) relative to fumed silica wherein large HPW crystallites are formed even at low HPW loadings. α -Pinene exhibits a volcano dependence on HPW loading over the SBA-15 support due to competition between the number and accessibility of acid sites to the non-polar reactant, with the superior acid site accessibility for HPW/SBA-15 conferring a 10-fold rate enhancement with respect to HPW/fumed silica and pure HPW. Monocyclic limonene and terpinolene products are favoured over polycyclic camphene and β -pinene by weaker polyoxometallate analogues over SBA-15.

© 2016 The Authors. Published by Elsevier B.V. This is an open access article under the CC BY license (<http://creativecommons.org/licenses/by/4.0/>).

1. Introduction

Bio-derived chemicals and fuels are urgently sought as sustainable alternatives to those currently derived from petrochemical refineries and related fossil fuel transformations. Catalytic routes to such products from lignocellulosic biomass, and plant or micro-organisms derived lipids and carbohydrates, have shown great recent promise in this regard. Heterogeneously catalysed transformations employing solid acids and bases, either alone, or in combination with one another and/or transition metal nanoparticles, are particularly attractive due to their (generally) superior chemical and thermal tolerance, lower cost, safer storage and handling, and amenability to continuous processing, compared with enzymatic or homogeneous analogues.

One important biogenic source of chemical building blocks is crude turpentine, obtained by distillation of resins during the mechanical pulping of pine trees. Turpentine is a mixture of terpenes, whose molecular structures derive from isoprene, and comprises predominantly α - and β -pinene, limonene, camphene, and terpinolene. The precise turpentine composition exhibits significant regional and seasonal variations, in addition to the nature of the tree species and extraction treatment employed [1]. Global

annual turpentine production is estimated to be 350,000 t [2], with the crude oil utilized as a solvent for dyes, paints and general organic synthesis. However terpene and terpenoids find application as high-value chemicals across the food, cosmetic, fragrance, pharmaceutical and biotechnology industries [3–5]. For example, *p*-cymene obtained through the dehydrogenation of α -pinene is becoming a key-compound for the production of synthetic fibres and antiseptics, in addition to a food flavorant; it is also a precursor to terephthalic acid [1,6,7], which finds application on the multi-million ton scale for polyester production (PET) [8]. *p*-Cymene can also be oxidised to *p*-cresol, which in turn is used to produce 2,6-di-*tert*-butyl-*p*-cresol (BHT), a light-resistant antioxidant with a wide range of applications [7,9–11].

α -Pinene isomerization offers routes to two important product families: monocyclic compounds such as limonene, terpinene, and terpinolene, and polycyclic compounds including camphene, β -pinene and tricyclene [12–16]. Camphene is a widely employed fragrance and solvent and a precursor to camphor, and additive in the formulation of insect repellents, explosives and plastics [1,7,13]. Limonene finds large scale application in the perfume and pharmaceutical industries of around 50,000 t annually [2]. The commercial isomerization of α -pinene is performed over TiO_2 catalyst at 100°C under autogeneous pressure, and delivers a broad product mixture with ~ 75 –80% total yield [17]. Despite the mild reaction conditions of this industrial process, its low conversion and selectivity requires significant advances to improve both atom

* Corresponding author.

E-mail address: a.f.lee@aston.ac.uk (A.F. Lee).

and energy efficiency. A wide range of alternative catalysts have been explored including alloys [14], clays [18,19], zeolites, [20,21] sulphated zirconia [16,22], Al-incorporated MCM-41 [23], and heteropolyacids (HPAs) [24–28]; with strong solid acids conferring improved conversion and selectivity [21,22,24,27,29].

HPAs are polyoxometalate inorganic cages which possess high Brønsted acid strengths (approaching the superacidic region) and tunable redox activity depending on the particular constituent elements. The Keggin form possesses the general formula $H_n(MX_{12}O_{40})^{n-}$, wherein M is the central atom within the cage and X the heteroatom; typically M is P or Si and X is W or Mo. The Keggin-type phosphotungstic acid $H_3PW_{12}O_{40}$ (HPW) with a formal primary unit of $PW_{12}O_{40}^{3-}$ and secondary unit of $H_3PW_{12}O_{40} \cdot 6H_2O$ [30], has attracted much interest due its strong Brønsted acidity and broad application to acid catalysed reactions [31–37]. However, bulk HPAs have a low surface area ($1\text{--}5\text{ m}^2\text{ g}^{-1}$), which hinders their performance as a heterogeneous catalyst, and hence there is an exigency to develop supported analogues [30,34,38–41]. For example, the encapsulation of phosphotungstic acid clusters within the cages of a MIL-101 MOF enhances selectivity towards the aldol self-condensation of cyclic ketones for high-density biofuels production [42]. HPW supported over MCM-41 has shown promise in α -pinene isomerization [43], albeit the small mesopore diameter of 2.5 nm and low maximum acid loading of 0.25 mmol g^{-1} , necessitated a high reaction temperature of $100\text{ }^\circ\text{C}$ and poor catalyst:substrate ratio to achieve significant activity. Hydrothermal processing of phosphotungstic acid has also been employed as a precursor to dope tungsten into the SBA-15 framework for high temperature ($130\text{ }^\circ\text{C}$) α -pinene isomerization, albeit without kinetic analyses [44].

Herein, we report on the dispersion and catalytic application of HPW over an ordered mesoporous SBA-15 support for α -pinene isomerization under mild conditions. The superior surface area and pore architecture of SBA-15 significantly increases the polyoxometalate dispersion and concomitant rate of isomerization over that attainable over a non-porous fumed silica support, while selectivity towards monocyclic limonene and terpinolene products is inversely proportional to acid strength.

2. Experimental

2.1. Catalyst synthesis

Two families of HPW catalysts were prepared via wet impregnation over silica supports, one a low area, fumed silica, and the other over a mesoporous SBA-15 ($900\text{ m}^2\text{ g}^{-1}$) synthesized according to our published methodology [45], with W loadings spanning 2–60 wt%. Wet impregnation was performed by dissolving the required amount of HPW (Aldrich, $\geq 99.9\%$) in 30 cm^3 methanol in a round-bottom flask at room temperature, followed by the addition of 1 g of either support. The mixture was stirred overnight and subsequently dried by solvent evaporation at room temperature. The resulting solid was ground and stored in air. Silicotungstic (HSiW, Aldrich, $\geq 99.9\%$) and phosphomolybdic (HPMo, Aldrich, ACS reagent) were also wet impregnated by the same methodology over the SBA-15 support as reference materials. All catalysts were used without subsequent thermal processing in order to retain water which is intrinsically linked to both the formation of the secondary structure of heteropolyacid clusters and their solid acidity.

2.2. Catalyst characterization

Elemental analysis was performed by XRF on a Bruker S8 Tiger. Thermogravimetric analysis was undertaken on a Mettler Toledo TGA/DSC 2 Star System between 40 and $800\text{ }^\circ\text{C}$ employing a ramp

rate of $10\text{ }^\circ\text{C min}^{-1}$ and Mettler Starl analysis software. Porosimetry measurements were conducted by N_2 physisorption on a Quantachrome Nova 4200e porosimeter with data analysis employing Novawin v11.0 software: samples were degassed at $120\text{ }^\circ\text{C}$ for 4 h prior to analysis by nitrogen adsorption at $-196\text{ }^\circ\text{C}$, with BET surface areas calculated over the range $P/P_0 = 0.05\text{--}0.35$ where a linear relationship was maintained, while pore size distributions were calculated using the BJH model from the desorption isotherm. DRIFT spectra were recorded on samples diluted to 5 wt% in KBr powder and stored at $70\text{ }^\circ\text{C}$ in *vacuo* prior to analysis. Spectra were acquired at $120\text{ }^\circ\text{C}$ on a Thermoscientific Nicolet iS50 FT-IR spectrometer equipped with a praying mantis environmental cell. XPS analysis was performed on a Kratos Axis HSi photo-electron spectrometer equipped with a charge neutralizer and magnetic focusing lenses, employing monochromatic Al $K\alpha$ radiation (1486.6 eV). Spectral fitting was performed using CasaXPS version 2.3.14, with energy referencing to the Si 2p peak at 100.1 eV, and W 4f spectra fitted with a common Doniach-Sunjic lineshape and FHMW. Powder XRD patterns were collected on a Bruker D8 Advance Diffractometer with a LynxEye high-speed strip detector using Cu $K\alpha$ (1.54 \AA) radiation, Ni filter and calibrated to quartz. Low angle data were collected between $2\theta = 0.45\text{--}8\text{ }^\circ$ and wide angle data between $2\theta = 10\text{--}80\text{ }^\circ$. Surface acidity was probed via ammonia chemisorption using a Quantachrome ChemBET3000 system with a MKS Minilab MS detector. Samples of 25–50 mg were outgassed at $150\text{ }^\circ\text{C}$ under flowing He ($150\text{ cm}^3\text{ min}^{-1}$) for 4 h in a quartz tube, prior to titration with 0.05 cm^3 pulses of 10 vol% NH_3 in He at $100\text{ }^\circ\text{C}$. Temperature programmed desorption (TPD) of ammonia saturated samples was performed under flowing He ($150\text{ cm}^3\text{ min}^{-1}$) between 100 and $800\text{ }^\circ\text{C}$ employing a ramp rate of $10\text{ }^\circ\text{C min}^{-1}$. Acid strengths were also determined through TPD of *n*-propylamine (Sigma Aldrich, $\geq 99\%$), wherein the desorption temperature of reactively-formed propene formed at acid sites is indicative of the solid acidity. Samples (10 mg) were impregnated with 0.5 cm^3 of propylamine and dried in *vacuo* at $40\text{ }^\circ\text{C}$ prior to analysis, with TPD performed on a Mettler Toledo TGA/DSC 2 Star System between 40 and $800\text{ }^\circ\text{C}$, using a ramp rate of $10\text{ }^\circ\text{C min}^{-1}$ and gas detection through a Pfeiffer Vacuum, ThermoStar MS. High resolution TEM images were obtained on an aberration corrected JEOL 2100-F microscope operated at 180 kV, with image analysis using ImageJ 1.41 software. Samples were dispersed in methanol and drop cast on 300-mesh carbon coated copper grids and dried under ambient conditions.

2.3. Catalyst testing

α -Pinene isomerization was performed in a Radleys Starfish reactor under air at $60\text{ }^\circ\text{C}$. 100 mg of catalyst was added to a reaction mixture of 126 mmol α -pinene (Sigma Aldrich, 98%) and 0.2 cm^3 of tetradecane (Sigma Aldrich, $\geq 99\%$) as an internal standard in a round-bottom flask, and stirred at 700 rpm for 6 h. Aliquots were sampled periodically, filtered and analysed by using a Bruker Scion 456-GC with an 8400 autosampler, fitted with a CP-5 column ($30\text{ m} \times 0.32\text{ mm} \times 0.25\text{ }\mu\text{m}$) and FID. Product yields were calculated from response factors determined from multi-point calibration curves. Conversion and selectivity were calculated according to the equations below, with activities calculated from the linear portion of reaction profiles, and all values are quoted $\pm 2\%$:

$$\text{Conversion}/\% = ([\text{mol}_{t=0} - \text{mol}_t]/\text{mol}_{t=0}) \times 100 \quad (1)$$

$$\text{Selectivity to product i}/\% = (\text{mol}_i/\sum \text{mol}_{\text{product}}) \times 100 \quad (2)$$

3. Results and discussion

3.1. Characterization

Successful supporting of HPW over both silica supports was first demonstrated by elemental analysis and powder XRD. Bulk W loadings, corrected for the amount of crystalline water measured by TGA according to a $H_3PW_{12}O_{40} \cdot 6H_2O$ stoichiometry [46,47], are shown for both families in Table 1, which span a similar range from 3 to 60 wt%. The parent SBA-15 and fumed silica supports show only a single broad diffraction peak around 23.2° and 22.9° respectively (Fig. 1). HPW/SBA-15 materials only exhibit the parent support reflection at the lowest W loadings, consistent with isolated Keggin clusters, with reflections characteristic of crystalline HPW emerging for loadings >9 wt%, presumably due to the nucleation of individual Keggin units, whose intensities increase and peak-widths decrease with W loading. Qualitatively similar trends were observed for the HPW/fumed silica family, albeit the emergence of HPW crystallites occurred at a lower loading, and the associated reflections were stronger (and sharper) than those for comparable loadings over the SBA-15 support. Together, these observations suggest that HPW is more highly dispersed over SBA-15 relative to fumed silica, as may be anticipated from their differing textural properties (see below). HPW volume averaged crystallite diameters derived from the Scherrer equation confirmed that HPW formed larger crystallites over fumed silica than SBA-15 for comparable loadings (Table 1). DRIFTS measurements of HPW/SBA-15 confirm the progressive evolution of characteristic phosphate, tungstate and silicate bands (Fig. S1) [48,49] which increase monotonically without saturating, indicating sub-monolayer growth [28]. It is worth noting that the reflections at low HPW loadings do not coincide perfectly with those of pure HPW. Similar observations have been made for phosphotungstic acid over a variety of oxide supports, attributed to a distortion of the tertiary structure at the interface [50].

Textural properties of the HPW materials shown in Fig. 2 also reveal important differences between the two silica supports. For HPW/SBA-15, the BET surface areas normalized per mass of silica (to compensate for the high density of incorporated HPW which would otherwise artificially distort surface areas at high loadings) exhibited only a small drop in surface area relative to the parent support (of around $140\text{ m}^2\text{ g}^{-1}$) for loadings ≤ 38 wt% in Fig. 2a. Higher HPW loadings induced a further significant loss of surface area, which fell to $500\text{ m}^2\text{ g}^{-1}$. In contrast, HPW impregnation over fumed silica had negligible impact on the normalized surface area for loadings ≤ 34 wt%, above which a significant increase in surface area was observed. This behaviour may be readily rationalized in terms of the different morphologies of the parent supports. In the case of SBA-15, the BET surface area is dominated by the internal porosity, and hence the incorporation of bulky HPW clusters is expected to induce pore blockage with a concomitant loss of mesopore volume and surface area. Fig. 2b confirms a systematic decrease in mesopore volume with HPW loading over SBA-15, although the corresponding BJH mesopore diameter remains unchanged ~ 5 nm except for the very highest loadings, coincident with the loss of internal porosity and surface area. These measurements suggest that HPW is highly dispersed within the SBA-15 mesopores for all but the highest loading, although a small fraction of pores are completely blocked even from low loadings, accounting for the partial loss of surface area and concomitant pore volume between 3 and 38 wt%. Fumed silica by contrast, possesses negligible internal surface area, and HPW deposition is therefore confined to the external support surface, wherein the extended three-dimensional crystallites (tertiary structure) formed at high loadings induce surface roughening and enhance the external surface area.

The nominal HPW surface coverage (θ) can be calculated according to Eq. (3), assuming a cross-sectional area of 1.44 nm^2 for a hexagonal close packed array of individual Keggin units [25,36,38]:

$$\theta = \frac{N_A \cdot \omega_{\text{HPW}}}{\text{MW}_{\text{HPW}}} \cdot \frac{1}{\text{SA}_{\text{support}}} \quad (3)$$

where N_A is the Avogadro number, ω_{HPW} is the mass fraction of HPW and $\text{SA}_{\text{support}}$ is the BET measured surface area per gram of support. The nominal HPW surface coverage increases linearly with loading over both supports, indicative of uniform HPW dispersion, but is considerably lower over SBA-15 for any given loading than for fumed silica, evidencing a higher dispersion.

Supported HPW nanostructures were also visualized by HRTEM (Fig. 3) at low and high loadings. Fig. 3a of the 3.2 wt% HPW/SBA-15 sample highlights the two-dimensional, parallel mesopore channels of the parent support, while an EDX line profile perpendicular to the channels demonstrates that HPW is concentrated within the mesopore voids. At these low loadings, HPW is incorporated into the mesoporous framework as uniformly dispersed, discrete Keggin units (consistent with the lack of crystallinity by XRD), each of approximately 1.2 nm diameter (Fig. 3b) in excellent agreement with the literature [36]. EDX confirmed a dramatic increase in the HPW concentration within the mesopores for the 55.7 wt% HPW/SBA-15 sample (Fig. 3c), although individual Keggin clusters could no longer be easily distinguished. In contrast, HPW was poorly dispersed over fumed silica, even at the lowest loading, with a broader range of particle sizes (1–2 nm) heterogeneously distributed over the amorphous, non-porous support (Fig. 3d). Higher HPW loadings result in the emergence of larger, irregular shaped clusters spanning 10–30 nm (Fig. 3e and f), consistent with porosimetry and XRD.

The thermal stability of silica supported HPW was studied by TGA (Fig. 4). Thermal decomposition proceeded in three distinct steps associated with the support and active HPW component [27]. A low temperature mass loss was observed for all HPW/SBA-15 samples between 90 and 100°C (highlighted blue) associated with the desorption of physisorbed water from the support. A second loss at 200°C (highlighted yellow) was only observed for high HPW loadings (≥ 38 wt% W) over SBA-15 (Fig. 4a inset). The appearance of this loss feature, which is attributed to the release of crystalline water from between individual Keggin clusters [51], indicates that a switcheroe occurs from isolated clusters <38 wt% W to larger agglomerates above this threshold. An additional weak and broad mass loss around 380°C arose from partial HPW decomposition and the subsequent reaction of acidic protons and structural oxygen [52]. The same three mass losses were observed from HPW/fumed silica, however a key difference was the appearance of crystalline water from all but the lowest 2.2 wt% sample, evidencing the formation of HPW agglomerates over fumed silica even at low loadings.

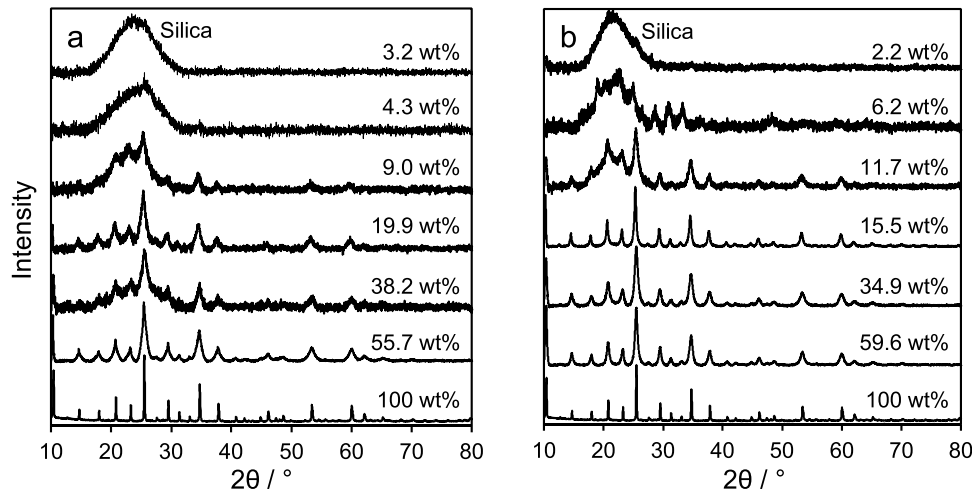
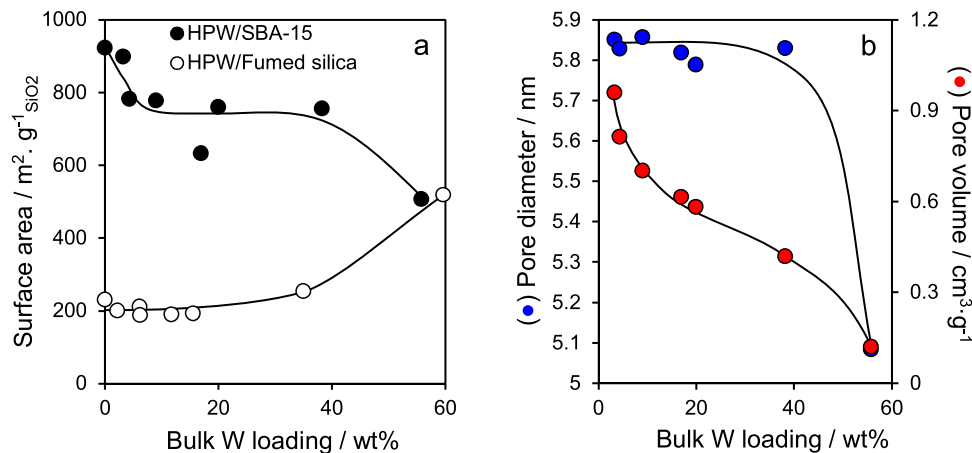
The evolution of surface HPW species over the SBA-15 support was further investigated through XPS (Fig. 5). Two distinct tungsten chemical species were observed for all HPW loadings: one associated with a $W\ 4f_{7/2}$ doublet at 32.5 eV, with a spin-orbit splitting of 2.15 eV, characteristic of bulk-like, three-dimensional HPW crystallites, and a second at 31.1 eV associated with a perturbed tungstate environment in HPW previously attributed to the interaction of terminal $W=O$ functions with surface silanols [24]. At low HPW loadings the ratio of interfacial:bulk W species was invariant ~ 0.4 , similar to the value of 0.33 reported previously for HPW over an amorphous porous silica [24], which was hypothesized to reflect a trimodal coordination mode for isolated clusters. The relative intensity of the bulk versus interfacial HPW species increases for W loadings >38.2 wt%, coincident with the formation of aggregated clusters and attendant crystalline water.

The solid acidity of silica supported HPW was evaluated through NH_3 chemisorption and subsequent TPD (Fig. S2). Table 2 reveals

Table 1

Surface coverage and crystallite size dependence of silica supported HPW.

HPW/SBA-15			HPW/fumed silica		
Bulk W loading/wt%	Particle size/nm	Surface coverage (θ)/ML	Bulk W loading/wt%	Particle size/nm	Surface coverage (θ)/ML
3.2	–	0.014	2.2	1.1	0.039
3.6	–	0.017	6.1	14.8	0.107
9	–	0.039	6.2	15.3	0.109
16.9	3.4	0.074	11.7	15.9	0.205
19.9	10.7	0.088	15.5	19.3	0.272
38.2	10.7	0.168	34.9	17.4	0.613
55.7	12.0	0.245	59.6	18.3	1.048

Unsupported $\text{H}_3\text{PW}_{12}\text{O}_{40}$ = 64.4 nm.**Fig. 1.** Powder XRD patterns for (a) HPW/SBA-15, and (b) HPW/fumed silica as a function of W loading, together with a pure HPW reference.**Fig. 2.** Variation of (a) surface areas of HPW/SBA-15 and HPW/fumed silica, and (b) mesopore diameter and mesopore volume of HPW/SBA-15 as a function of bulk W loading.**Table 2**

Acid site densities of silica supported HPW.

HPW/SBA-15		HPW/fumed silica	
Bulk W loading/wt%	Acid loading/mmol g ⁻¹	Bulk W loading/wt%	Acid loading/mmol g ⁻¹
3.2	0.15	2.2	0.06
3.6	0.23	6.1	0.16
9	0.24	6.2	0.16
16.9	0.27	11.7	0.19
19.9	0.29	15.5	0.20
38.2	0.30	34.9	0.20
55.7	0.54	59.6	0.26

Unsupported $\text{H}_3\text{PW}_{12}\text{O}_{40}$ = 1 mmol g⁻¹.

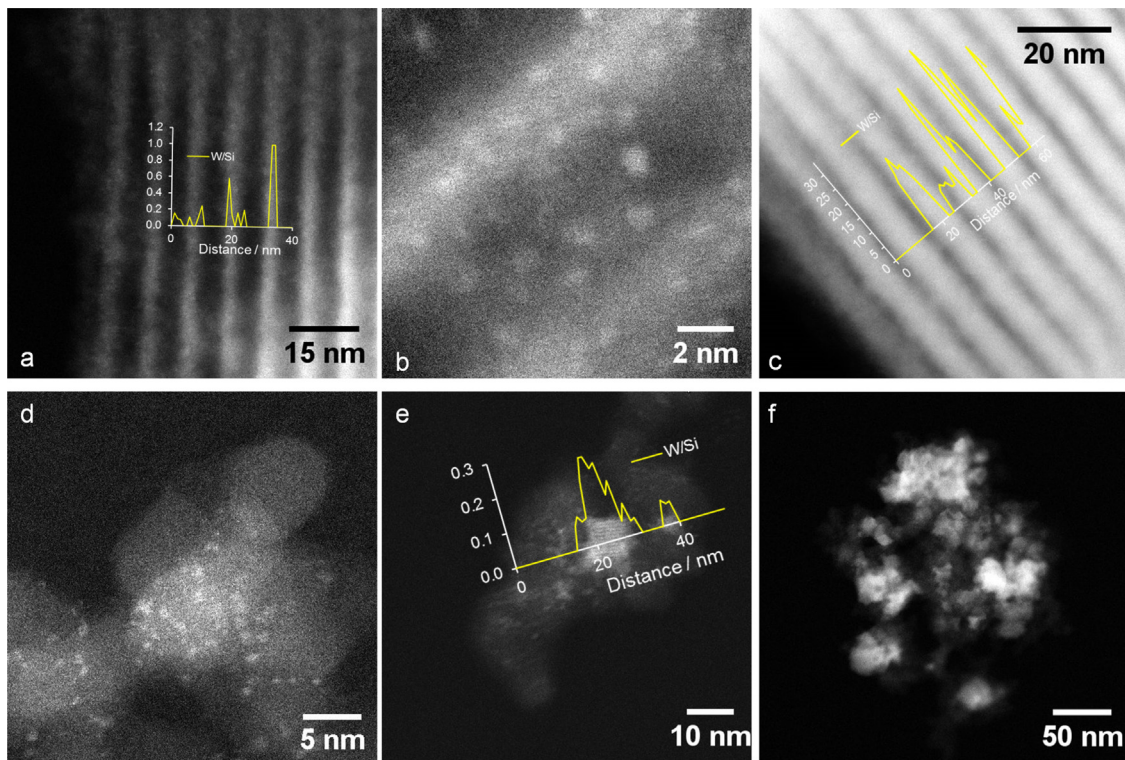


Fig. 3. HRTEM dark-field images of (a and b) 3.2 wt% HPW/SBA-15, (c) 55.7 wt% HPW/SBA-15, (d) 2.2 wt% HPW/fumed silica, (e) 19.2 wt% HPW/fumed silica, (f) 59.6 wt% HPW/fumed silica. Insets show corresponding EDX atomic ratio line profiles.

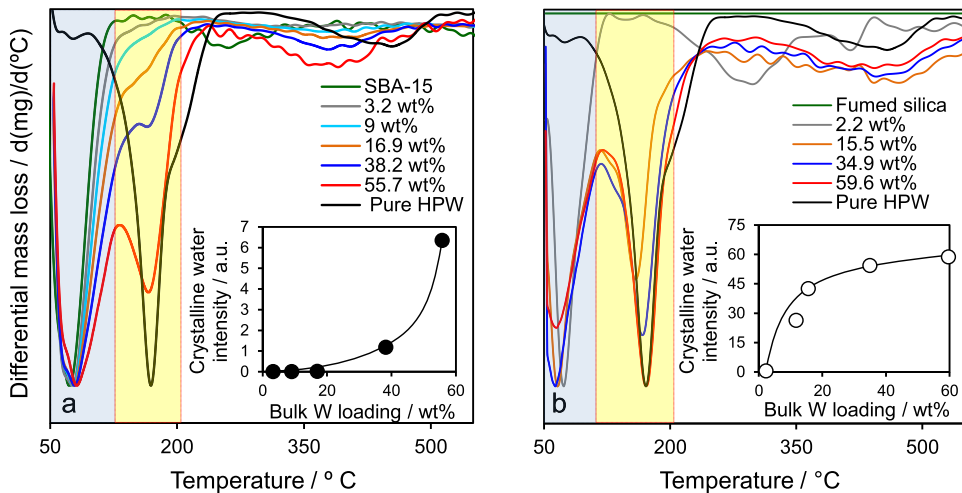


Fig. 4. Differential thermal analysis profiles for (a) HPW/SBA-15, and (b) HPW/fumed silica as a function of bulk W loading. Insets shows integrated desorption peak for crystalline water. (For interpretation of the references to color in the text, the reader is referred to the web version of this article.)

that SBA-15 supported HPW possess significantly higher acid site densities relative to equivalent loadings over fumed silica, reflecting the far higher dispersion of the former and hence accessibility of acid sites to the base probe. Ammonia TPD spectra exhibited three distinct desorption peaks for both supports, centred around 200, 420 and 610 °C. The first coincides with the loss of crystalline water, and hence is attributed to ammonia coordinated to water either between Keggin units, or at the interface between isolated Keggin clusters and the silica surface, and is loading invariant suggesting a constant acid strength. The intermediate and high temperature desorptions are associated respectively with ammonia coordinated to the charge balancing H^+ of individual Keggin units [32,51,53], and their subsequent thermal transformation to tungstate and phos-

phate species, accompanied by the liberation of reactively-formed protons [52,54–56]; these are unlikely to play a role in low temperature catalytic processes, wherein the primary Keggin structure and entrained water remain intact. Integrated peak intensities for the 200 °C desorption (Fig. S2) show an approximately linear increase in the number of associated acid sites for the HPW/SBA-15 with W loading up to 38.2 wt%, confirming that these sites are associated with highly dispersed isolated or two-dimensional arrays of HPW clusters, above which they reach a plateau. In contrast, HPW/fumed silica possesses less than one third the number of these low temperature acid sites, whose intensity passes through a maximum at only 11.7 wt%, presumably due to the early onset of bulk crystallite formation and reduced acid site accessibility.

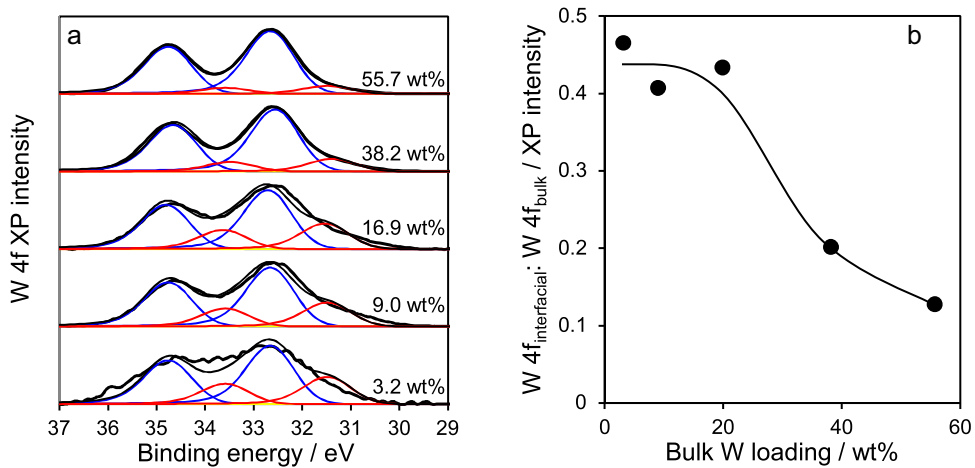


Fig. 5. (a) Background-subtracted W 4f XP spectra of HPW/SBA-15, and (b) ratio of integrated interfacial:bulk HPW as a function of bulk W loading.

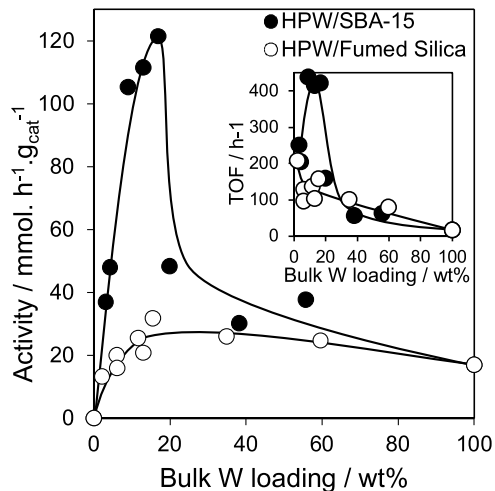


Fig. 6. Specific activity for α -pinene isomerization over HPW/SBA-15 and HPW/fumed silica at 60 °C as a function of bulk W loading. Insets show corresponding TOFs.

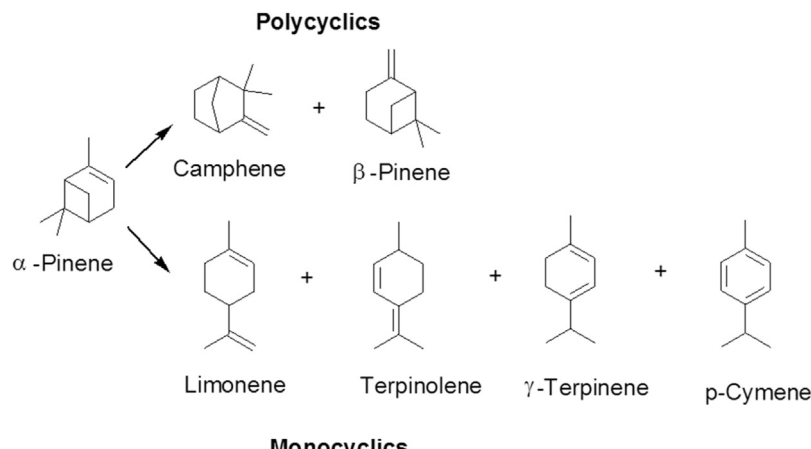
3.2. α -Pinene isomerization

The heterogeneously catalysed isomerization of α -pinene is sensitive to both the acid site density and strength, with two principal reaction pathways identified illustrated in **Scheme 1** [22,24]. Ring opening reactions yield monocyclic products such as limonene and terpinolene, while ring rearrangement favours camphene and β -pinene.

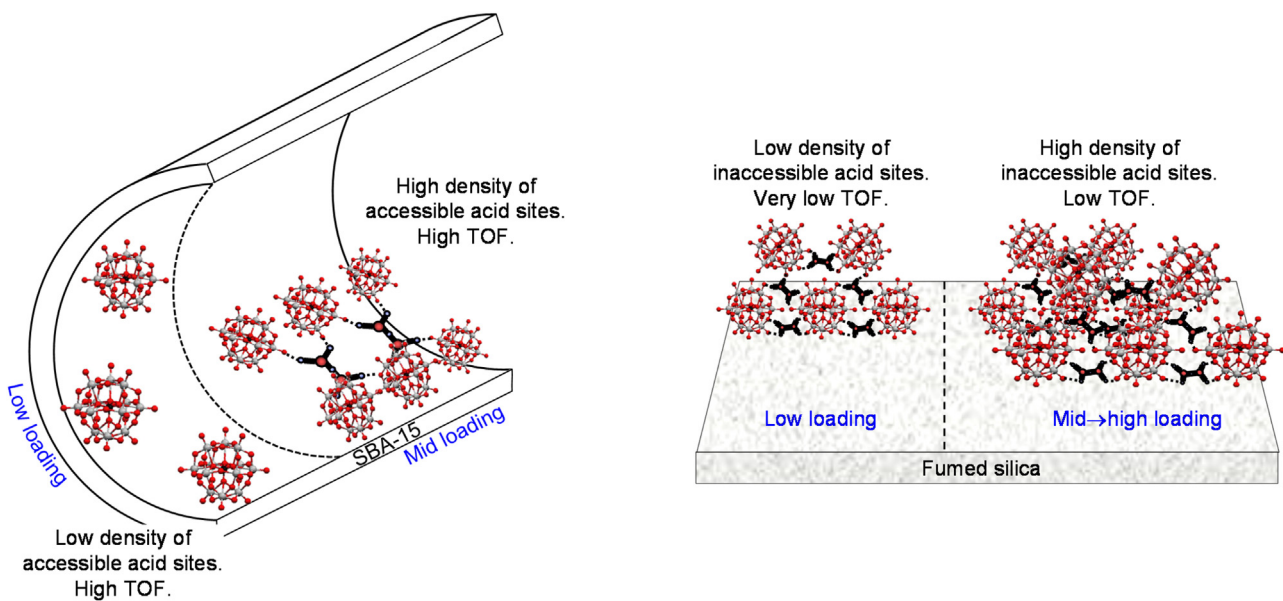
Fumed silica and SBA-15 were inert towards α -pinene under our mild reaction conditions. All HPW/fumed silica catalysts exhibited poor conversions <10% (Fig. S3) and activities of approximately 20 mmol h⁻¹ g_{cat}⁻¹ (Fig. 6) which were essentially loading independent and comparable to unsupported pure HPW. In comparison, HPW/SBA-15 samples exhibited good conversions between 10 and 40%, and a strong volcano dependence of activity on W loading, but with a maximal rate almost an order of magnitude higher than over the fumed silica support of 121 mmol h⁻¹ g_{cat}⁻¹. The correspondence between the acid sites associated with crystalline/interfacial water and initial rate is weaker, with rates falling at high loadings wherein the 200 °C ammonia desorption state attains a plateau. The dramatically enhanced specific activity of the HPW/SBA-15 catalysts for this non-polar liquid phase transformation can be readily attributed to the superior dispersion of HPW, as either isolated Keggin clusters (visualized by HRTEM in Fig. 3b) or low dimensional

HPW arrays (implicit from porosimetry, thermal analysis and XRD) within the SBA-15 mesopores, and hence accessibility of acid sites within a HPW monolayer across the silica surface. The majority of acid sites for HPW/fumed silica are localized within larger and likely three-dimensional HPW crystallites and hence only accessible to α -pinene at the very lowest loadings. Corresponding Turnover Frequencies (TOFs) determined by normalising the specific activity to the acid site densities from ammonia chemisorption (Table 2), mirror the rate dependence on loading over both supports. The increase in apparent TOF between ~3 wt% (from 200 h⁻¹) to ~15 wt% W (440 h⁻¹) suggests that isolated Keggin units are less active than small/low dimensional aggregates, as may be anticipated since the former lacks acid sites associated with water held within the secondary heteropolyacid structure, while the formation of tertiary HPW structures at loadings >20 wt% W contributes acid sites which are poorly accessible to the non-polar terpene reactant resulting in a significant fall in the mean TOF; α -pinene isomerization thus appears predominantly confined to acid sites at the interface with silica or low dimensional HPW aggregates. The structural evolution and corresponding reactivity of HPW over both supports is summarized in **Scheme 2**. It is interesting to note that Fig. 6 shows the maximum (mass-normalized) catalytic activity for SBA-15 supported HPW was attained for bulk W loadings between 10 and 20 wt%, whereas Fig. S2c shows that the number of weakly acidic sites (characterized by a 200 °C ammonia desorption in Fig. S2a) rises monotonically to a plateau >20 wt%. However, there is no discrepancy between these two observations. First, Fig. S2c shows that the increase in catalyst density for W loadings >20 wt% is not accompanied by an increase in the number of weak acid sites, and hence a decrease in the mass-normalized rate of α -pinene isomerization (per gram of catalyst) >20 wt% W is entirely expected (same number of active sites but in a denser material). Second, activity will be proportional to the number of accessible active sites, and the textural properties of HPW/SBA-15 catalysts show a significant loss of surface area, mesopore diameter and mesopore volume for W loadings above 20 wt% (Fig. 2). The evolution of accessible weak acid sites with W loading can be estimated by plotting the product of the intensity of 200 °C acid sites from Fig. S2 with select textural properties from Fig. 2; Fig. S4 reveals that the resulting parameters are a good predictor of the loading dependent activities in Fig. 6, reproducing the volcano profile and maximum around 20 wt% W.

Both catalyst families exhibited similar (loading invariant) product selectivities of ~55% to monocyclic products (Fig. S5), reflecting their common temperature for the first ammonia desorption state and hence acid strength. Since product selectivity is sensitive to acid strength, as illustrated below, the support dependence on TOF



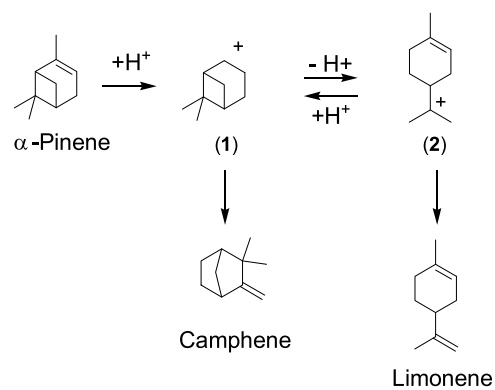
Scheme 1. Principal products of α -pinene isomerization.



Scheme 2. Cartoon depiction of loading dependent structure-reactivity behaviour of HPW supported on high area, mesoporous SBA-15 versus non-porous, fumed silica.

for HPW/SBA-15 does not appear attributable to a difference in the strength of interfacial acid sites; rather, it likely reflects the poorer accessibility of acid sites in larger HPW crystallites to α -pinene relative to polar ammonia, and hence is an artefact of normalization to the latter.

In order to elucidate the relationship between product selectivity and acid strength, α -pinene isomerization was also explored over two related Keggin polyoxometallates supported on SBA-15, silicotungstic (HSiW) and phosphomolybdc (HPMo) acids, at 9 wt% heteroatom loadings; literature studies employing Hammett indicators, pyridine and ammonia calorimetry and TPD indicate these are weaker solid acids than HPW [24,31,35,51,54–58]. Propylamine chemisorption over these three SBA-15 supported heteropolyacids, and the subsequent desorption temperature for reactively-formed propene (Fig. 7a) confirmed that their acid strength decreases in the order HPW > HSiW > HPMo, mirroring their TOFs (Fig. 7b). As the acid strength decreases, so the selectivity towards polycyclic products (camphene and β -pinene) falls at the expense of monocyclics (predominantly limonene and terpinolene). This close correlation between acid strength and ring opening versus rearrangement pathways supports current postulates for the isomerization mechanism. It is generally accepted that the first step in α -pinene



Scheme 3. Acid catalysed routes to polycyclic versus monocyclic products from α -pinene.

isomerization is its protonation to generate a pinyll cation (1) as shown in Scheme 3 [9,43]. The pinyll cation is believed to be a precursor to polycyclic camphene via isomerization to an isobornyl cation and subsequent deprotonation, however (1) can also depro-

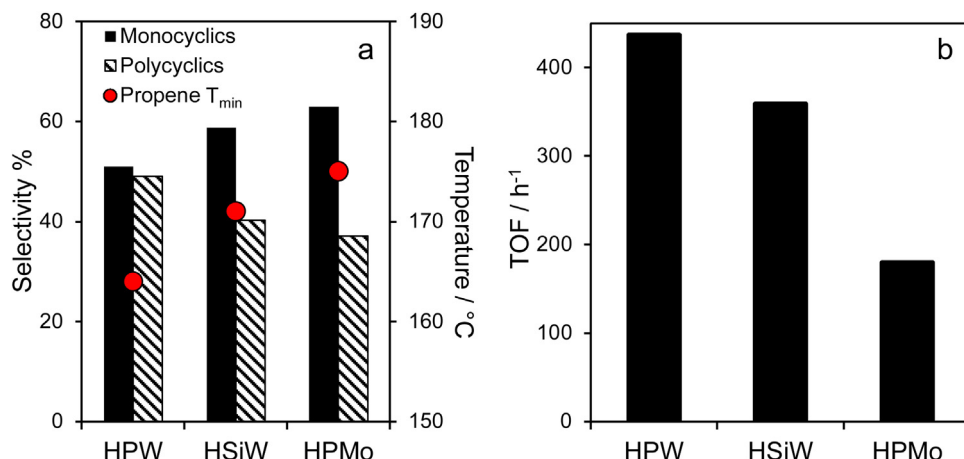


Fig. 7. (a) Correlation between α -pinene selectivity after 6 h reaction, and the acid strength of heteropolyacids supported on SBA-15 measured by the desorption temperature for reactively-formed propene following propylamine chemisorption, and (b) corresponding TOFs. Catalysts compared at a common 9 wt% W (or Mo) loading.

tonate to form a *p*-menthenyl cation (**2**) which is the precursor to monocyclic products such as limonene (and terpinolene and α -terpinene via further isomerization to the tertiary *p*-menthenyl cation). Our results suggest that the weaker acid HPMo/SBA-15 facilitates deprotonation of (**1**) to (**2**) and consequently favours the more thermodynamically stable single ring structure [31]. However, in the presence of the stronger acid HPW/SBA-15, the equilibrium appears displaced towards (**1**) favouring polycyclics.

4. Conclusions

The physicochemical properties of a family of mesoporous SBA-15 supported $\text{H}_3\text{PW}_{12}\text{O}_{40}$ (HPW) catalysts have been characterised by bulk and surface sensitive probes as a function of acid loading and compared with fumed silica analogues. Structurally, the parent Keggin unit is preserved over both supports, however the higher area SBA-15 support permits the stabilisation of high concentrations of isolated and/or low dimensional polyoxometallate clusters throughout the mesopores, which present a high density of accessible Brønsted acid sites. In contrast, fumed silica favours the formation of large HPW crystallites even at low loadings, which are inhomogeneously dispersed across the external surface and exhibit poorer acid site densities. Low temperature solventless isomerization of α -pinene exhibits a volcano dependence on the HPW loading over SBA-15, reflecting a balance between increasing acid site density, and the decreasing accessibility of these acid sites within the polar environment of extended Keggin aggregates formed at higher loadings, to the non-polar terpene. The superior dispersion and acidity of HPW/SBA-15 confers a 10-fold rate enhancement for the optimum 9 wt% bulk W loading towards the low temperature solventless isomerization of α -pinene with respect to HPW/fumed silica and unsupported HPW, and a corresponding increase in the apparent TOF per accessible acid site. Comparative studies of SBA-15 supported HPW, HSiW and HPMo reveal that α -pinene selectivity to monocyclic limonene and terpinolene products (relative to polycyclics camphene and β -pinene) is inversely proportional to the solid acid strength.

Acknowledgements

We thank the EPSRC (EP/K000616/2; EP/K014749/1 and EP/M005186/1), Royal Society, and British Council under the Global Innovation Initiative for the GB3-net project, for financial support.

Appendix A. Supplementary data

Supplementary data associated with this article can be found, in the online version, at <http://dx.doi.org/10.1016/j.apcatb.2016.06.064>.

References

- [1] M. Colonna, C. Berti, M. Fiorini, E. Binassi, M. Mazzacurati, M. Vannini, S. Karanam, *Green Chem.* 13 (2011) 2543–2548.
- [2] M. Golets, S. Ajaikumar, J.-P. Mikkola, *Chem. Rev.* 115 (2015) 3141–3169.
- [3] J.L. Bicas, A.P. Dionísio, G.M. Pastore, *Chem. Rev.* 109 (2009) 4518–4531.
- [4] C. Lorenzo, A. Eugenio, *Recent Patents Food Nutr. Agric.* 3 (2011) 9–16.
- [5] C.C.C.R. de Carvalho, M.M.R. da Fonseca, *Biotechnol. Adv.* 24 (2006) 134–142.
- [6] B.L. Arthur, N.W., Michael, C.R. Morris, *Oxidation process for preparation of terephthalic acid*, Google Patents, 1953.
- [7] C. Berti, E. Binassi, M. Colonna, M. Fiorini, G. Kannan, S. Karanam, M. Mazzacurati, I. Odeh, M. Vannini, *Bio-Based Terephthalate Polyesters*, 2010, US 9024060 B2.
- [8] R.J. Sheehan, *Ullmann's Encyclopedia of Industrial Chemistry*, Wiley-VCH Verlag GmbH & Co. KGaA, 2000.
- [9] M. Golets, S. Ajaikumar, M. Mohn, J. Wärnå, S. Rakesh, J.P. Mikkola, *J. Catal.* 307 (2013) 305–315.
- [10] H. Fiege, *Ullmann's Encyclopedia of Industrial Chemistry*, Wiley-VCH Verlag GmbH & Co. KGaA, 2000.
- [11] H. Fiege, H.-W. Voges, T. Hamamoto, S. Umemura, T. Iwata, H. Miki, Y. Fujita, H.-J. Buysch, D. Garbe, W. Paulus, *Ullmann's Encyclopedia of Industrial Chemistry*, Wiley-VCH Verlag GmbH & Co. KGaA, 2000.
- [12] A. Stanislaus, L.M. Yeddanapalli, *Can. J. Chem.* 50 (1972) 61–74.
- [13] A. Corma, S. Iborra, A. Velty, *Chem. Rev.* 107 (2007) 2411–2502.
- [14] V. Wystrach, L. Barnum, M. Garber, *J. Am. Chem. Soc.* 79 (1957) 5786–5790.
- [15] F. Ebmeyer, *J. Mol. Struct.: Theochem.* 582 (2002) 251–255.
- [16] N. Comelli, E. Ponzi, M. Ponzi, *J. Am. Oil Chem. Soc.* 82 (2005) 531–535.
- [17] A. Severino, J. Vital, L.S. Lobo, in: M. Guisnet, J. Barbier, J. Barrault, C. Bouchouche, D. Duprez, G. Péro, C. Montassier (Eds.), *Studies in Surface Science and Catalysis*, Elsevier, 1993, pp. 685–692.
- [18] N. Besün, F. Özkan, G. Gündüz, *Appl. Catal. A: Gen.* 224 (2002) 285–297.
- [19] S. Findik, G. Gündüz, *J. Am. Oil Chem. Soc.* 74 (1997) 1145–1151.
- [20] K. Hensen, C. Mahaim, W.F. Hölderich, *Appl. Catal. A: Gen.* 149 (1997) 311–329.
- [21] A. Severino, A. Esculcas, J. Rocha, J. Vital, L.S. Lobo, *Appl. Catal. A: Gen.* 142 (1996) 255–278.
- [22] M.A. Ecormier, A.F. Lee, K. Wilson, *Microporous Mesoporous Mater.* 80 (2005) 301–310.
- [23] J.-J. Zou, N. Chang, X. Zhang, L. Wang, *ChemCatChem* 4 (2012) 1289–1297.
- [24] A.D. Newman, D.R. Brown, P. Siril, A.F. Lee, K. Wilson, *Phys. Chem. Chem. Phys.: PCCP* 8 (2006) 2893–2902.
- [25] A.M. Alsalme, P.V. Wiper, Y.Z. Khimyak, E.F. Kozhevnikova, I.V. Kozhevnikov, *J. Catal.* 276 (2010) 181–189.
- [26] A. Alsalme, E.F. Kozhevnikova, I.V. Kozhevnikov, *Appl. Catal. A: Gen.* 390 (2010) 219–224.
- [27] K. Narasimharao, D. Brown, A. Lee, A. Newman, P. Siril, S. Tavener, K. Wilson, *J. Catal.* 248 (2007) 226–234.
- [28] A.D. Newman, A.F. Lee, K. Wilson, N.A. Young, *Catal. Lett.* 102 (2005) 45–50.
- [29] M.A. Ecormier, K. Wilson, A.F. Lee, *J. Catal.* 215 (2003) 57–65.
- [30] N. Mizuno, M. Misono, *Chem. Rev.* 98 (1998) 199–218.
- [31] M.N. Timofeeva, *Appl. Catal. A: Gen.* 256 (2003) 19–35.

[32] B.B. Bardin, R.J. Davis, M. Neurock, *J. Phys. Chem. B* 104 (2000) 3556–3562.

[33] Y. Zhang, Z. Du, E. Min, *Catal. Today* 93–95 (2004) 327–332.

[34] T. Okuhara, N. Mizuno, M. Misono, *Appl. Catal. A: Gen.* 222 (2001) 63–77.

[35] Y. Izumi, R. Hasebe, K. Urabe, *J. Catal.* 84 (1983) 402–409.

[36] M.S. Kaba, I.K. Song, M.A. Barreau, *J. Phys. Chem. B* 106 (2002) 2337–2342.

[37] M. Misono, *Chem. Commun.* (2001) 1141–1152.

[38] T. Okuhara, N. Mizuno, M. Misono, in: W.O.H.D.D. Eley, G. Bruce (Eds.), *Advances in Catalysis*, Academic Press, 1996, pp. 113–252.

[39] K. Inumaru, T. Ishihara, Y. Kamiya, T. Okuhara, S. Yamanaka, *Angew. Chem. Int. Ed.* 46 (2007) 7625–7628.

[40] I.V. Kozhevnikov, *Chem. Rev.* 98 (1998) 171–198.

[41] Y. Zhou, G. Chen, Z. Long, J. Wang, *RSC Adv.* 4 (2014) 42092–42113.

[42] Q. Deng, G. Nie, L. Pan, J.-J. Zou, X. Zhang, L. Wang, *Green Chem.* 17 (2015) 4473–4481.

[43] G. Nie, J.-J. Zou, R. Feng, X. Zhang, L. Wang, *Catal. Today* 234 (2014) 271–277.

[44] C.H. Wu, H.Q. Liu, C.F. Zhuang, G.B. Du, in: M.Z. Abdullah (Ed.), *Mechanical Engineering, Materials and Energy* Iii, Trans Tech Publications Ltd., Stafa-Zurich, 2014, pp. 134–137.

[45] C.M.A. Parlett, D.W. Bruce, N.S. Hondow, A.F. Lee, K. Wilson, *ACS Catal.* 1 (2011) 636–640.

[46] A. Micek-Ilnicka, *J. Mol. Catal. A: Chem.* 308 (2009) 1–14.

[47] L. Marosi, E. Escalona Platero, J. Cifre, C. Otero Arean, *J. Mater. Chem.* 10 (2000) 1949–1955.

[48] K. Pamín, A. Kubacka, Z. Olejniczak, J. Haber, B. Sulikowski, *Appl. Catal. A: Gen.* 194–195 (2000) 137–146.

[49] T. Blasco, A. Corma, A. Martínez, P. Martínez-Escalano, *J. Catal.* 177 (1998) 306–313.

[50] G. Marci, E. Garcia-Lopez, M. Bellardita, F. Parisi, C. Colbeau-Justin, S. Sorgues, L.F. Liotta, L. Palmisano, *Phys. Chem. Chem. Phys.* 15 (2013) 13329–13342.

[51] B.B. Bardin, S.V. Bordawekar, M. Neurock, R.J. Davis, *J. Phys. Chem. B* 102 (1998) 10817–10825.

[52] B.W.L. Southward, J.S. Vaughan, C.T. Oconnor, *J. Catal.* 153 (1995) 293–303.

[53] B.B. Bardin, R.J. Davis, *Appl. Catal. A: Gen.* 200 (2000) 219–231.

[54] J. Highfield, J. Moffat, *J. Catal.* 88 (1984) 177–187.

[55] E. Lalik, A. Micek-Ilnicka, A. Groszek, A. Bielański, *Phys. Chem. Chem. Phys.* 5 (2003) 3606–3609.

[56] L.C. Jozefowicz, H.G. Karge, E. Vasilyeva, J.B. Moffat, *Microporous Mater.* 1 (1993) 313–322.

[57] S. Ganapathy, M. Fournier, J.F. Paul, L. Delevoye, M. Guelton, J.P. Amoureux, *J. Am. Chem. Soc.* 124 (2002) 7821–7828.

[58] L. Pesaresi, D.R. Brown, A.F. Lee, J.M. Montero, H. Williams, K. Wilson, *Appl. Catal. A: Gen.* 360 (2009) 50–58.